

Experimental Study of High Frame Rate Imaging with Limited Diffraction Beams

Jian-yu Lu, *Member, IEEE*

Abstract—Limited diffraction beams have a large depth of field and have many potential applications. Recently, a new method (Fourier method) was developed with limited diffraction beams for image construction. With the method and a single plane wave transmission, both 2D (two-dimensional) and 3D (three-dimensional) images of a very high frame rate (up to 3750 frames/s for a depth of 200 mm in biological soft tissues) and a high signal-to-noise ratio (SNR) can be constructed with relatively simple and inexpensive hardware. If limited diffraction beams of different parameters are used in both transmission and reception and transducer aperture is shaded with a cosine function, high-resolution and low-sidelobe images can be constructed with the new method without montage of multiple frames of images [the image quality is comparable to that obtained with a transmit-receive (two-way) dynamically focused imaging system]. In this paper, the Fourier method was studied with both experiment and computer simulation for 2D B-mode imaging. In the experiment, two commercial broadband 1D array transducers (48 and 64 elements) of different aperture sizes (18.288 and 38.4 mm) and center frequencies (2.25 and 2.5 MHz) were used to construct images of different viewing sizes. An ATS539 tissue-equivalent phantom of an average frequency-dependent attenuation of 0.5 dB/MHz/cm was used as a test object. To obtain high frame rate images, a single plane wave pulse (broadband) was transmitted with the arrays. Echoes received with the arrays were processed with both the Fourier and conventional dynamic focusing (delay-and-sum) methods to construct 2D B-mode images. Results show that the quality (resolution and contrast) of constructed images is virtually identical for both methods, except that the Fourier method is simpler to implement. Both methods have also a similar sensitivity to phase aberration distortions. Excellent agreement among theory, simulation, and experiment was obtained.

I. INTRODUCTION

LIMITED DIFFRACTION BEAMS were first developed in 1941 by Stratton [1]. Theoretically, these beams can propagate to an infinite distance without spreading. In practice, when these beams are produced with a finite aperture and energy, they have a large depth of field. Because of this attractive property, limited diffraction beams have been further studied by many investigators in optics [2]–[4], electromagnetics [5], and acoustics [6], [7].

Limited diffraction beams have also been studied for both medical and nonmedical applications, such as, medical imaging [8]–[11], tissue characterization [12], volumet-

ric imaging [13], estimation of transverse velocity of blood flow [13]–[15], high-speed digital wireless telecommunications [16], and nondestructive evaluation (NDE) of industrial materials [17]. Families of limited diffraction beams such as X waves (the waves have an “X-like” shape in the plane along the wave axis) [18], [19] were discovered and applied to medical imaging [20]–[23]. Electronic steering of these beams with 1.5-dimensional (1.5D) or two-dimensional (2D) arrays were studied [24]. Methods for constructing new limited diffraction beams from existing diffracting or limited diffraction beams were developed [25]–[27]. In addition, methods for reducing sidelobes of these beams were also developed, such as, summation-subtraction [28], deconvolution [29], and using newly developed bowtie beams [30], [31]. Some of the subjects are reviewed in [10], [21].

Another type of beam that also has a large depth of field is called localized waves or “focus wave mode” discovered first in 1983 by Brittingham [32]. These waves have been further studied by many investigators in electromagnetics [33]–[36]. Localized waves are different from limited diffraction beams because their shapes deform as they propagate. Properties of these beams such as sidelobes are essentially the same as those of limited diffraction beams when the bandwidth of these beams are limited and realizable with a typical medical ultrasonic transducer [21], [37].

Based on the studies of limited diffraction beams, recently, a new method has been developed for both 2D and 3D imaging at a very high frame rate [38]. In this method, a plane wave pulse (broadband) is used to illuminate an object to be constructed. Waves scattered from the object are received with a 1D (one-dimensional) (for 2D B-mode imaging, where image plane is in parallel with transducer axis) or 2D (for 3D imaging) array transducer. The received signals are weighted with limited diffraction beams of different parameters to produce multiple A-lines simultaneously. From the temporal Fourier transform of these A-lines, the Fourier transform of the object is obtained, and thus an image of the object can be constructed with a 2D (for 2D B-mode imaging) or 3D (for 3D imaging) inverse spatial Fourier transform. From the image construction, there are several important features with this method: First, because only one transmission is necessary, the image frame rate is very high for both 2D and 3D imaging. Assume that the speed of sound in biological soft tissues is 1500 m/s, the highest frame rate possible is about 3750 frames/s for a typical depth of 200 mm in the human body. The very high frame rate will substantially reduce motion artifacts of fast moving objects

Manuscript received October 26, 1996; accepted August 8, 1997. This work was supported in part by grants CA 54212, CA 43920, and HL 60301 from the National Institutes of Health.

The author is with the Department of Bioengineering, The University of Toledo, Toledo, OH 43606 (e-mail: jilu@eng.utoledo.edu).

such as the mitral valve leaflet. The high frame rate can also be used to achieve high contrast with incoherent processings such as spatial or multiple frame compounding. Second, because the entire array aperture is used to produce a plane wave, the total transmit power is high and the wave will not spread within 200 mm with conventional medical transducers. This means that the energy will not diverge over a large depth of field and thus signal-to-noise ratio (SNR) is high. Third, because fast Fourier transforms (FFT) can be used in the image construction, the system is relatively simple and inexpensive as compared to conventional dynamically focused beamformers attempting to achieve high frame rates. For example, to construct a 3D object having N_x , N_y , and N_z points along the x , y , and z axes, respectively, the amount of computation of the Fourier method is proportional to $N_x \times N_y \times N_z \times \log_2 N_z$, where N_z is usually a large number [10680 if RF (radio frequency) signals are digitized at 40 megasamples/s over a 200 mm range]. With conventional dynamic focusing (delay-and-sum [39]) method, the amount of computation is proportional to $N_x \times N_y \times N_z \times N_{x_1} \times N_{y_1}$ plus delay and interpolation operations, where N_{x_1} and N_{y_1} are number of elements of a 2D array in the x and y directions, respectively. If $N_{x_1} = N_{y_1} = 128$ (128×128 2D array), the ratio between operations required by the dynamic focusing and the Fourier methods is approximately $(N_{x_1} \times N_{y_1}) / \log_2 N_z \approx 1224$. Fourth, because of the potential high frame rate, RF signals can be used to construct 2D or 3D flow vector images with speckle tracking [40] without decorrelation. This will increase the accuracy of estimation of blood flow volume, which is a significant higher dimensional parameter used in diagnostic ultrasound. Even with conventional color flow imaging methods [41], the accuracy of velocity estimation will increase with this new technology because more samples can be used for calculation while maintaining a high frame rate. Fifth, the quality (contrast and resolution) of images constructed with the Fourier method is as high as that obtained with the conventional dynamic focusing method using the same transmit beam (see results of this paper). In addition, both methods have a similar sensitivity to phase aberration distortions [42]. If limited diffraction beams of different parameters are used in both transmission and reception [38], [69] and a cosine shading is applied to the transducer aperture, the Fourier method will have a lower frame rate but a high image quality (high resolution and low sidelobe). To achieve such quality with conventional transmit-receive (two-way) dynamic focusing, multiple frames of images must be combined with a montage resulting in a very low frame rate.

It should be noticed that beam steering is not necessary to construct high frame rate images with the Fourier method. However, if a large field of view is desirable, both transmit and receive beams can be steered electronically [24] to increase the image area. In this case, image frame rate may be reduced by a few folds, depending on the size of transducer aperture (a larger aperture is desirable to achieve a higher frame rate, but it will be limited by the

sizes of acoustic windows in human body). However, the constructed images at different steering angles can be used for compounding to increase the contrast of the overlapping areas (see Fig. 8). In the case where limited diffraction beams are used in both transmission and reception, beam steering is not needed at all to construct images that have a field of view larger than the size of a transducer aperture [69].

To understand the advantages of the Fourier method, let's study the following example of a conventional beam forming. Assuming that a transmit beam is focused to form a thin beam around its focal length and a receive beam is dynamically focused, a 3D image can be obtained by scanning both the transmit and receive beams line by line within a volume. To produce each A-line, the beams require approximately $267 \mu\text{s}$ to reach a depth of 200 mm in biological soft tissues. To insonate a 3D volume, there would be approximately 128×128 A-lines or more requiring an elapsed time of 4.37 s or a resultant frame rate of 0.229 frames/s. This is not acceptable for cardiac or blood flow imaging. To increase the frame rate, a wider beam and multiple dynamic focusing beamformers instead of a thin beam illuminating a small area must be used. The frame rate will increase linearly with the number of beamformers. However, for each dynamic focusing beamformer, there must be 128×128 channels if a 128×128 2D array is to be used. Notably, the number of parallel receivers cannot be greatly increased due to the complexity of the system. In short, it is not practical to produce a 3D image at very high frame rates with any conventional dynamic focusing beamformer. For 2D B-mode imaging, the conventional beamformer achieves a frame rate of about 30 frames/second and the frame rate drops with the number of beams transmitted at different focal distances to overcome the short depth of field of focused beams. In cardiovascular imaging, multiple transmits are usually not used. To increase the image frame rate to 3750 for a depth of 200 mm, a broad illumination beam must be used and approximately 128 conventional B-scan machines would need to work in parallel. This demonstrates that even for 2D B-mode imaging where only a 1D array is used and if the number of channels were 128, it is difficult, if not impossible, to substantially increase the frame rate at a depth of 200 mm using a conventional beamformer. For color flow imaging, because multiple frames are required to obtain flow information (i.e., the more frames used, the more accurate the measured blood velocity), frame rates will be further reduced with conventional beamformers. In current clinical practice to maintain or increase the frame rate, one either reduces the depth or limits the viewing angle which reduces diagnostic attributes. Therefore, a new approach, such as the Fourier method, must be developed to increase the frame rate for cardiac and blood flow imaging.

Several multidimensional ultrasound imaging solutions have been proposed to increase image frame rate. The first was a 3D imaging system developed at Duke University where a wide transmit beam is used to illuminate an area that contains 16 to 32 conventional dynamically focused

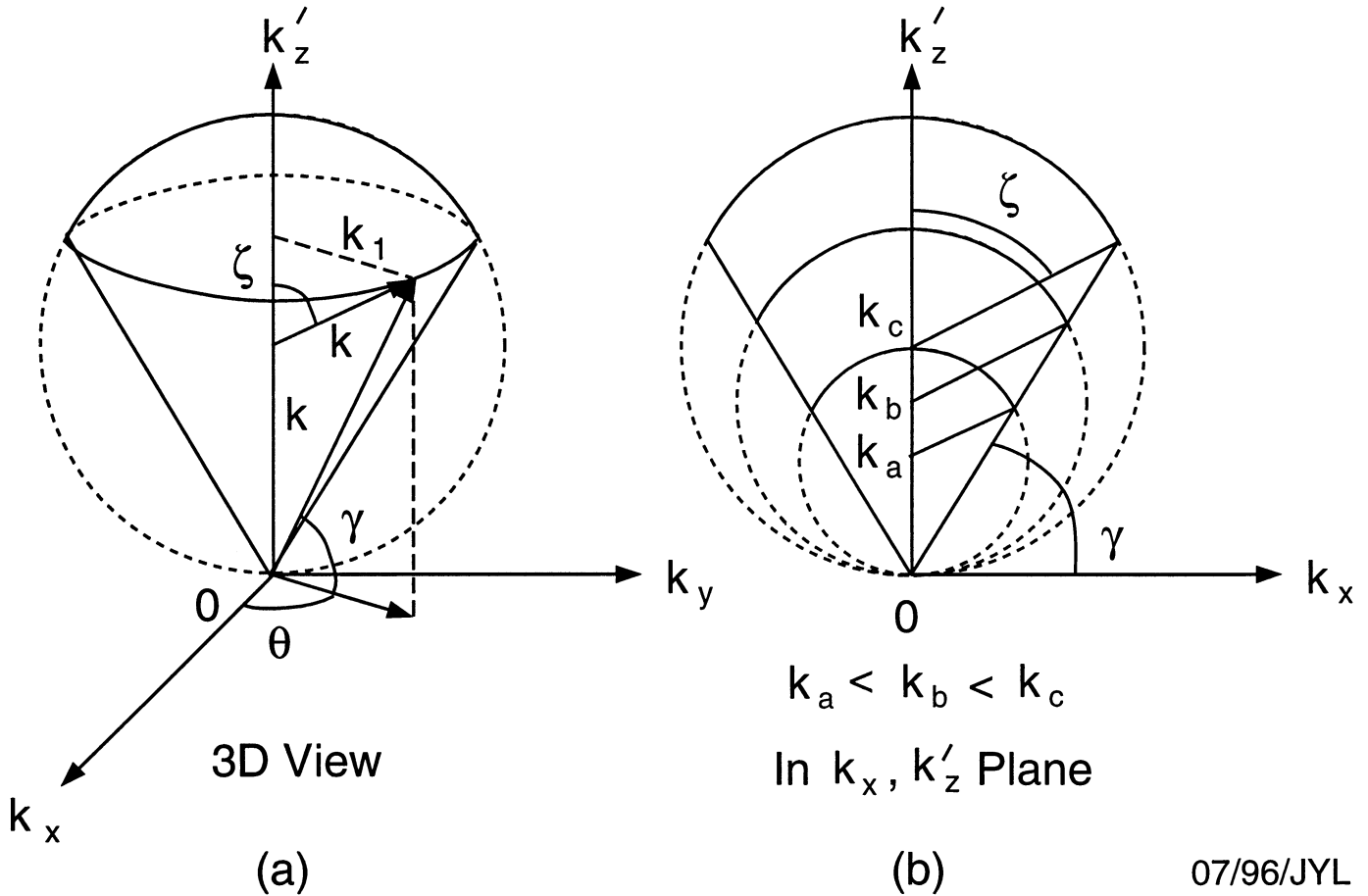


Fig. 1. Spatial Fourier-domain coverage of a pulse-echo imaging system where a plane wave pulse (broadband) is used in transmission, and limited diffraction beams of different parameters are used in reception. (a) 3D view and (b) the view at $k_x - k'_z$ plane ($k_y = 0$). k_a , k_b , and k_c are three examples of the wavenumber, k , to show how the Fourier space coverage is increased with k .

receive beams [43]–[45]. This system is limited: First, the frame rate is increased by only about 32 times, which is still low even for conventional imaging. For color flow Doppler imaging or dynamic focusing in transmission, the frame rate must be further reduced. Second, there must be 16 to 32 multichannel dynamically focused beamformers to process receive signals in parallel leading to a very complex system. Although this problem is partially avoided by using a principal beamformer and multiple approximate beamformers (explosocan [43]), the approximate beamformers produce phase errors that distort objects and degrade image quality as the receive beams scan from one angle to another. Therefore, the number of approximate beamformers and thus the frame rate is difficult to be further increased. Third, to cover all 16 to 32 receive beams uniformly, the transmit beam must be wide enough and thus the transmit aperture will be reduced by at least 16 to 32 times which in turn decreases transmit energy leading to a low SNR (signal-to-noise ratio) at greater depths.

Other methods are based on synthetic aperture and holographic concepts [46]. For example, a diverging transmit beam can be used to illuminate an object. Backscatter signals can be processed with a delay-and-sum (dynamic focusing) algorithm [39] where for each point in the ob-

ject, its distance to the elements of a receiver array is determined and appropriate delays are added to the receive signals so that they can be summed constructively for a particular point. For this method to work, RF signals are required and thus a high sampling rate is needed to avoid signal aliasing and delay quantization errors. As mentioned above, this requires a huge computational power to obtain a frame rate approximating 3750 and results in a very complex system. In addition, the energy density of a diverging wave is inversely proportional to the square of distance and thus will have an extremely low SNR in biological soft tissues. Ylitalo and Ermert [47] have proposed a backpropagation Fourier method. This method has a very low frame rate in 3D imaging because more than 10,000 transmissions are required to obtain a frame of image. This method also suffers from low SNR because strongly diverged transmit beams have to be used to increase lateral resolution. In addition, the method is based on the holographic concept, where monochromatic illumination is desirable which reduces axial resolution of images. Soumekh [48] has proposed a phased-array Fourier method. This method also suffers from low frame rate in 3D imaging because beams must be transmitted in multiple directions to construct a frame of image. The method may also have high sidelobes

unless a shading function such as a cosine function is applied to both the transmit and receive apertures. Methods for 3D real-time imaging using coded transmissions and matrix inversions also have been proposed [49], [50]. These methods suffer from problems similar to those of the synthetic aperture (diverging beams) and the delay-and-sum (a large amount of computations).

It is worth noting that construction of images with backscattered signals has been studied by many investigators [51]–[53]. Norton and Linzer [51] have suggested using a point source on a 2D array to transmit and receive sequentially to construct images. As discussed above, this method will suffer from slow frame rate and low SNR, and thus is not suitable for *in vivo* study of biological soft tissues for a valid diagnosis. Ultrasound tomography also can use backscattered signals to construct images but requires a 360° rotation around body [54]–[56]. This limits application because of the acoustic obstructions within the human body. In addition, tomography is slow, the systems are complex, and images suffer from misregistration due to significant changes of speed of sound at different viewing angles.

In this paper, an experiment for 2D B-mode imaging was performed to verify the theoretical image construction formulas derived from limited diffraction beams. 3D imaging will be studied in the future when 2D arrays are more available and affordable. In the experiment, an ATS539 tissue-equivalent phantom¹ and commercial 1D array transducers were used, and a plane wave pulse (broadband) was transmitted with the arrays. Results of the Fourier method were compared to those obtained with the delay-and-sum algorithm (dynamic focusing) and with computer simulations.

The paper is organized as follows. The theory of the Fourier method pertinent to the experiment is reviewed in Section II. Experiment, simulation, and their results will be described in Section III. A brief discussion and conclusion will be given in Sections IV and V, respectively.

II. THEORETICAL PRELIMINARIES

In the following, the theory of the Fourier method and 2D and 3D image construction formulas pertinent to the experimental study will be briefly reviewed. Details can be found in [38].

A. X Waves and Limited Diffraction Array Beams

From X waves (see equation 12 in [18]), one obtains limited diffraction array beams [13], [25], [26]. X waves are

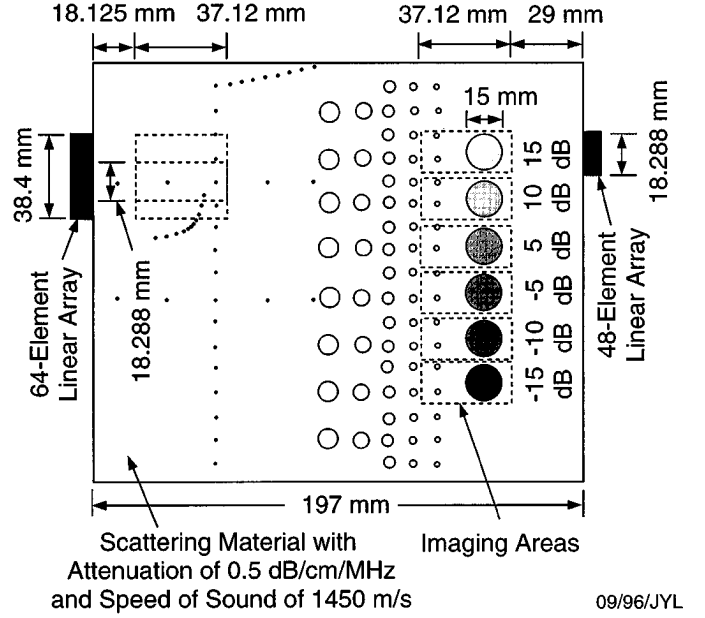


Fig. 2. A cross-section of an ATS539 multipurpose rubber-based tissue equivalent phantom for 2D B-mode imaging. The phantom is composed of line scatterers, grayscale cylindrical objects, and anechoic cylindrical objects. All the objects are embedded in a background of random scatterers. The contrasts of the grayscale objects are ranged from -15 dB to $+15$ dB relative to the background. Rectangular boxes are areas where 2D B-mode images are to be constructed.

given by:

$$\begin{aligned} \Phi_{X_n}(\vec{r}, t) &= \Phi_{X_n}(r, \phi, z - c_1 t) \\ &= e^{in\phi} \int_0^{\infty} B(k) J_n(kr \sin \zeta) e^{-k[a_0 - i \cos \zeta (z - c_1 t)]} dk, \end{aligned} \quad (1)$$

where $n = 0, 1, 2, \dots$, is the “order” of the waves, $\vec{r} = (r, \phi, z)$ represents a spatial point in the cylindrical coordinates, t is time, r is radial distance, ϕ is polar angle, z is the axial distance, $c_1 = c / \cos \zeta$ is the phase velocity of X waves, $k = \omega / c$ is the wave number, $\omega = 2\pi f$ is the angular frequency, f is the temporal frequency, c is the speed of sound or light, $\zeta (0 \leq \zeta < \pi/2)$ is the Axicon angle of X waves (the angle between X branches and a plane perpendicular to the direction of the wave propagation) [18], [57]–[59], $J_n(\cdot)$ is the n th-order Bessel function of the first kind, $B(k)$ is any well-behaved function that could represent the transfer function of a practical acoustic transducer or electromagnetic antenna, and a_0 is a constant that determines the fall-off speed of the high-frequency components of X waves.

Summing the X waves in (1) over the index, n , we obtain broadband limited diffraction array beams [13], [25], [26] that remain limited diffraction solutions to the isotropic-

¹ATS Laboratories, Inc., Bridgeport, CT.

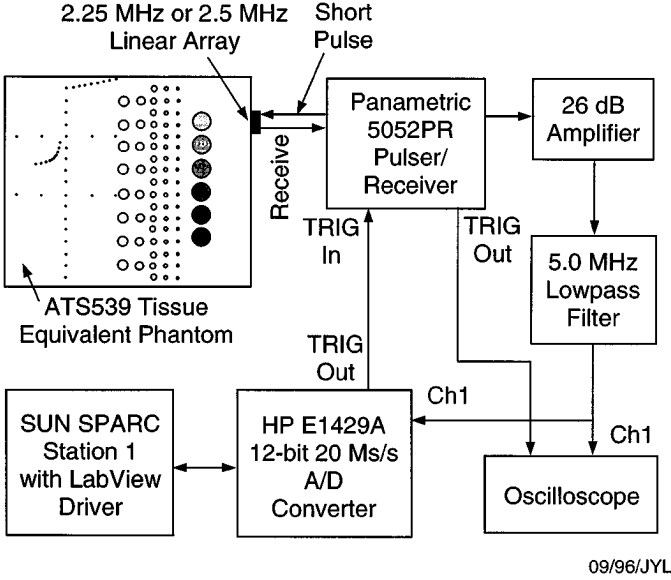


Fig. 3. A block diagram of the experiment.

homogeneous wave equation:

$$\begin{aligned} \Phi_{\text{Array}}(\vec{r}, t) &= \sum_{n=-\infty}^{\infty} i^n e^{-in\theta} \Phi_{X_n}(r, \phi, z - c_1 t) \\ &= \int_0^{\infty} B(k) \left[\sum_{n=-\infty}^{\infty} i^n J_n(kr \sin \zeta) e^{in(\phi - \theta)} \right] \\ &\quad \times e^{-k[a_0 - i \cos \zeta (z - c_1 t)]} dk, \end{aligned} \quad (2)$$

where $0 \leq \theta < 2\pi$ is a free parameter and the subscript "Array" represents "array beams". Because of the following equality (see p. 620 in [60]),

$$\sum_{n=-\infty}^{\infty} i^n J_n(kr \sin \zeta) e^{in(\phi - \theta)} = e^{i(kr \sin \zeta) \cos(\phi - \theta)}, \quad (3)$$

the array beams can be written as [38]:

$$\begin{aligned} \Phi_{\text{Array}}(\vec{r}, t) &= \frac{1}{2\pi} \int_0^{\infty} T(k) e^{ik_x x + ik_y y + ik_z z} e^{-i\omega t} dk \\ &= \frac{1}{2\pi} \int_{-\infty}^{\infty} T(k) H(k) e^{ik_x x + ik_y y + ik_z z} e^{-i\omega t} dk, \end{aligned} \quad (4)$$

where

$$\frac{T(k)H(k)}{c} e^{ik_x x + ik_y y + ik_z z}, \quad (5)$$

is the Fourier transform (spectrum) of the array beams in terms of time,

$$H\left(\frac{\omega}{c}\right) = \begin{cases} 1, & \omega \geq 0 \\ 0, & \omega < 0 \end{cases} \quad (6)$$

is the Heaviside step function [61], $T(k) = 2\pi B(k)e^{-ka_0}$, and

$$\begin{cases} k_x = k \sin \zeta \cos \theta = k_1 \cos \theta \\ k_y = k \sin \zeta \sin \theta = k_1 \sin \theta \\ k_z = k \cos \zeta = \sqrt{k^2 - k_1^2} \geq 0 \end{cases}, \quad (7)$$

and where

$$k_1 = \sqrt{k_x^2 + k_y^2} = k \sin \zeta. \quad (8)$$

B. Image Constructions

3D Image construction: Let's assume that a 3D object, $f(\vec{r})$ (reflection coefficient), is composed of randomly positioned point scatterers embedded in a uniform background supporting a constant speed of sound and a broadband circular 2D array transducer is excited to produce a plane wave pulse (broadband) that is expressed as follows (obtained from equation 4 in [18]):

$$\begin{aligned} P(z - ct) &= \frac{1}{2\pi} \int_{-\infty}^{\infty} A(k) e^{ik(z-ct)} dk \\ &= \frac{1}{2\pi} \int_{-\infty}^{\infty} A(k) e^{ikz} e^{-i\omega t} dk, \end{aligned} \quad (9)$$

where

$$\frac{A(k)e^{ikz}}{c} \quad (10)$$

is the temporal spectrum of the wave. If the same array transducer is used as a receiver and is weighted to produce a limited diffraction array beam response with the parameters k_x and k_y , the received signal for the waves scattered from point scatterers within the volume, V , of the object is given by the following convolution [use (5) and (10)]:

$$\begin{aligned} R_{k_x, k_y, k'_z}(t) &= \int_V f(\vec{r}) [P(z - ct) * \Phi_{\text{Array}}(\vec{r}, t)] d\vec{r} \\ &= \frac{1}{2\pi} \int_{-\infty}^{\infty} \frac{A(k)T(k)H(k)}{c} \left[\int_V f(\vec{r}) e^{ik_x x + ik_y y + ik'_z z} d\vec{r} \right] \\ &\quad \cdot e^{-i\omega t} dk = \frac{1}{2\pi} \int_{-\infty}^{\infty} \frac{A(k)T(k)H(k)}{c} F(k_x, k_y, k'_z) e^{-i\omega t} dk, \end{aligned} \quad (11)$$

where "*" represents the convolution with respect to time and where $k'_z = k + k_z$, and $F(k_x, k_y, k'_z)$ is the Fourier transform of the object function. This uses the fact that the spectrum of the convolution of two functions is equal to the product of the spectra of the functions and the imaging system is linear (approximately true in medical ultrasonic imaging). Notice that k_x and k_y in (4) or (5) can be determined directly from the weighting parameters of limited diffraction array beams.

From (11), a relationship between the temporal Fourier transform (spectrum) of the received signal, $\tilde{R}_{k_x, k_y, k'_z}(\omega)$, and a band-limited version of the spatial Fourier transform of the object function, $F_{\text{BL}}(k_x, k_y, k'_z)$, is obtained:

$$F_{\text{BL}}(k_x, k_y, k'_z) = c^2 H(k) \tilde{R}_{k_x, k_y, k'_z}(\omega), \quad (12)$$

where $H(k)$ indicates that only positive values of k are used and thus it can be applied to either side of the equation (for the convenience of presentation, it is used with $\tilde{R}_{k_x, k_y, k'_z}(\omega)$), and

$$F_{\text{BL}}(k_x, k_y, k'_z) = A(k)T(k)F(k_x, k_y, k'_z), \quad (13)$$

where the subscript ‘‘BL’’ means ‘‘band-limited’’. If the combined transmit and receive transfer function $A(k)T(k) \equiv 1$ (infinite bandwidth), $F_{\text{BL}}(k_x, k_y, k'_z) = F(k_x, k_y, k'_z)$ is an exact Fourier transform of the object function. In practical systems, $A(k)T(k)$ is always band-limited and thus it can be assumed, for example, to be proportional to the Blackman window function [18], [64]:

$$W(k) = \begin{cases} 0.42 - 0.5 \cos \frac{\pi k}{k_0} + 0.08 \cos \frac{2\pi k}{k_0}, & 0 \leq k \leq 2k_0 \\ 0, & \text{otherwise} \end{cases}, \quad (14)$$

where $k_0 = 2\pi f_0/c$ and f_0 is the center frequency. The -6 -dB bandwidth of $W(k)$ is about 81% of its center frequency which is typical for modern medical ultrasonic transducers. If the object function, $f(\vec{r})$, is real, which is the case in most applications, we have:

$$F(-k_x, -k_y, -k'_z) = F^*(k_x, k_y, k'_z), \quad (15)$$

where the superscript ‘‘*’’ means complex conjugate. In this case, the spatial Fourier transform of the object function in the lower Fourier space ($k'_z < 0$) is also known. With the inverse spatial Fourier transform [61], one can approximately construct 3D images directly from (12) [38]. In addition, using the 3D inverse spatial Fourier transform expression [61] and variable substitutions in (7), one obtains a close-form formula for 3D image construction (see [38] for details):

$$f(\vec{r}) \approx \frac{c^2}{(2\pi)^3} \int_0^\infty k^2 dk \int_{-\pi}^\pi d\theta \int_0^{\pi/2} \sin \zeta (1 + \cos \zeta) d\zeta \tilde{R}'_{k, \zeta, \theta}(\omega) \cdot e^{-ikr \sin \zeta \cos(\phi - \theta) - ik(1 + \cos \zeta)z}, \quad (16)$$

where $\tilde{R}'_{k, \zeta, \theta}(\omega) = \tilde{R}_{k_x, k_y, k'_z}(\omega)$ and the approximation in (16) is due to the fact that all physical systems are band-limited and only part of the Fourier space is known from backscattered data because the aperture of a transducer is finite [Fig. 1(a)].

2D B-Mode imaging: 2D imaging is a special case of 3D. In the following, 2D B-mode imaging formulas will be derived. Formulas for 2D C-mode (image plane is perpendicular to the transducer axis) imaging are given in [38]. 2D C-mode imaging requires a 2D array transducer and will not be discussed in this paper.

In 2D B-mode imaging, objects are assumed to be two-dimensional, i.e., object function does not change in the elevation direction, y , or, the object function is given by $f^{(2)}(\vec{r}) = f^{(2)}(x, z)$, where the superscript ‘‘(2)’’ means ‘‘2D B-mode’’. In this case, it is not necessary to weight array transducers in the y direction, and thus a 1D, instead of 2D array transducer can be used.

From (4), broadband layered array beams can be derived by setting the free parameter, k_y , to zero [13], [25]–[26]:

$$\Phi_{\text{Layer}}(x, z, t) = \frac{1}{2\pi} \int_{-\infty}^{\infty} T(k)H(k)e^{ik_x x + ik_z z} e^{-i\omega t} dk, \quad (17)$$

where the subscript ‘‘Layer’’ represents ‘‘layered array beams’’, $k'_z = k + k_z$, and where

$$\begin{cases} k_x = k \sin \zeta \\ k_z = \sqrt{k^2 - k_x^2} = k \cos \zeta \geq 0 \end{cases} \quad (18)$$

is a special case of (7) with $\theta \equiv 0$.

With a broadband plane wave (9) insonification, from (11), we obtain the received signal

$$\begin{aligned} R_{k_x, k'_z}^{(2)}(t) &= \frac{1}{2\pi} \int_{-\infty}^{\infty} \frac{A(k)T(k)H(k)}{c} \\ &\times \left[\int_S f^{(2)}(x, z) e^{ik_x x + ik'_z z} dx dz \right] e^{-i\omega t} dk \\ &= \frac{1}{2\pi} \int_{-\infty}^{\infty} \frac{A(k)T(k)H(k)}{c} F^{(2)}(k_x, k'_z) e^{-i\omega t} dk, \end{aligned} \quad (19)$$

where $F^{(2)}(k_x, k'_z)$ is a spatial Fourier transform of $f^{(2)}(x, z)$ and ‘‘S’’ is an area in the x - z plane. [Because $k'_z \geq k$ ($k \geq 0$), the spatial Fourier transform of $f^{(2)}(x, z)$ is known only in the area shown in Fig. 1(b).]

If $f(\vec{r})$ is also a function of y , the $f^{(2)}(x, z)$ in (19) represents an effective 2D object function that is given by:

$$f^{(2)}(x, z) = \int_{-\infty}^{\infty} f(\vec{r}) dy. \quad (20)$$

In most B-scan systems, beams are focused with a lens in the elevation direction (y direction), the slice thickness is quite small at focus and the effective 2D object function (20) can be written as follows:

$$f^{(2)}(x, z) \approx f(x, y_0, z) d_y, \quad (21)$$

where y_0 is the center plane of the slice defined by the elevation focus and d_y is the slice thickness (notice that the focusing in the y direction will not affect the layered array beams in the x direction [13], [14]).

From (19), it follows:

$$F_{\text{BL}}^{(2)}(k_x, k'_z) = A(k)T(k)F^{(2)}(k_x, k'_z) = c^2 H(k) \tilde{R}_{k_x, k'_z}^{(2)}(\omega), \quad (22)$$

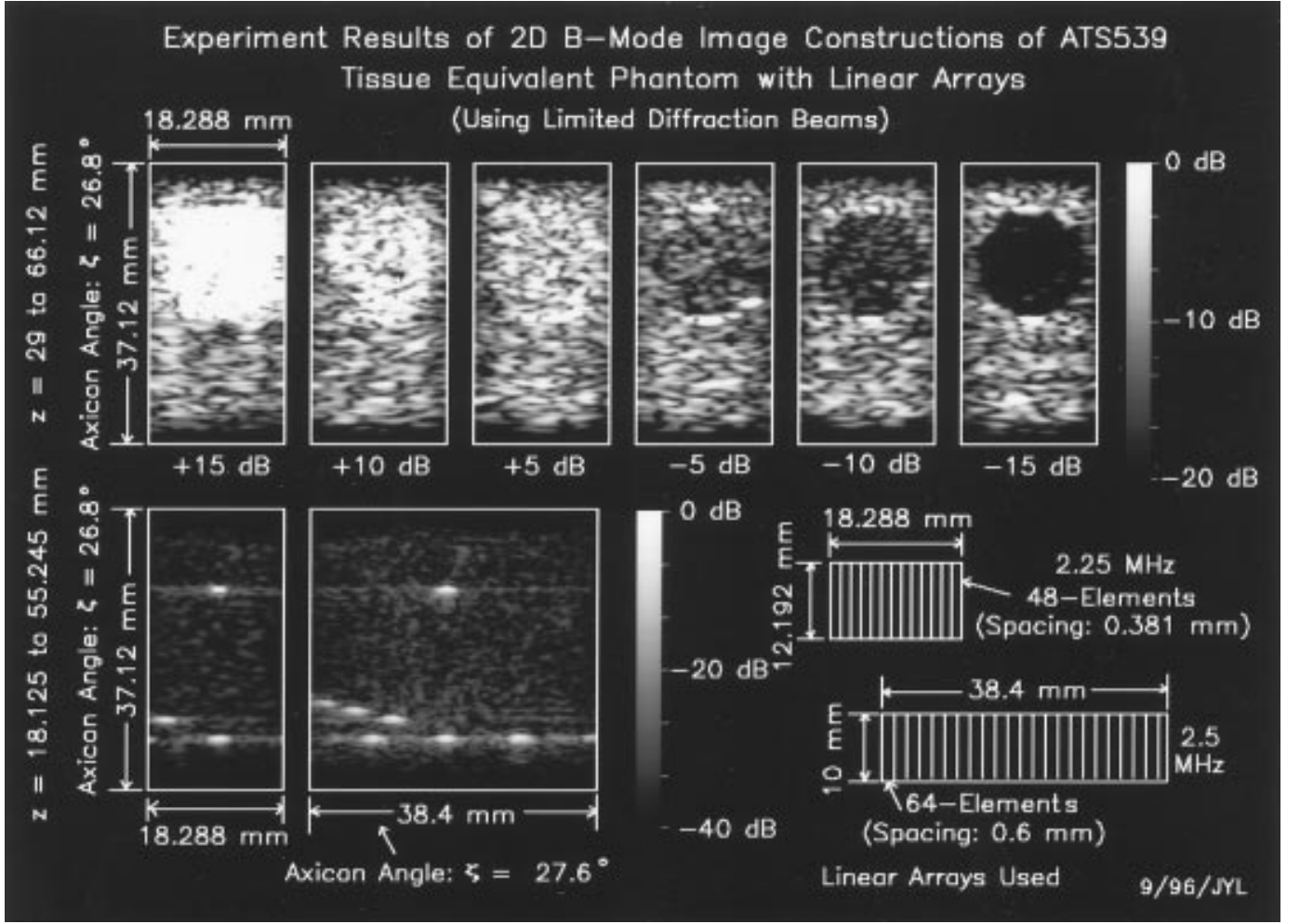


Fig. 4. 2D B-mode images of an ATS539 tissue-equivalent phantom constructed with experimental data and with the Fourier method developed from limited diffraction beams. In the experiment, a single plane wave pulse (broadband) is used in transmission to achieve a very high frame rate. Panels in the top row correspond to constructed images of the cylindrical grayscale objects. Panels in the bottom row are images of line objects. The dimensions and the locations of the images in the phantom are shown in both this figure and Fig. 2. Dark areas near the top and bottom of each image are resulted from Blackman windows added to A-lines near these regions to reduce potential aliasing in image constructions.

where $\tilde{R}_{k_x, k'_z}^{(2)}(\omega)$ is the temporal Fourier transform of $R_{k_x, k'_z}^{(2)}(t)$. From (22), 2D B-mode images can be constructed approximately with an inverse 2D spatial Fourier transform.

A close-form formula similar to (16) for the construction of 2D B-mode images can also be obtained [38]:

$$f^{(2)}(x, z) \approx \frac{c^2}{(2\pi)^2} \int_0^\infty k dk \int_0^{\pi/2} (1 + \cos \zeta) d\zeta \times \tilde{R}_{k, \zeta}^{(2)'}(\omega) e^{-ikx \sin \zeta - ik(1 + \cos \zeta)z}, \quad (23)$$

where $\tilde{R}_{k, \zeta}^{(2)'}(\omega) = \tilde{R}_{k_x, k'_z}^{(2)}(\omega)$ and the approximation “ \approx ” is due to the finite bandwidth and finite transducer aperture of the system [Fig. 1(b)].

III. EXPERIMENT, SIMULATION, AND THEIR RESULTS

The Fourier method can be used for 3D imaging (see (11), (12), and (16)). However, 3D imaging requires a 2D array that will complicate the experiment. In the following, an experiment for 2D B-mode imaging with 1D arrays is performed to verify the Fourier method. Results of computer simulation for 3D imaging are given in [38].

In the experiment, an ATS539 multipurpose rubber-based (speed of sound is 1450 m/s at 23°C) tissue-equivalent phantom was used. The dimension of a cross-section of the phantom is shown in Fig. 2 where boxes of dotted lines are areas for image constructions. The phantom is composed of line targets and cylindrical objects consisting of point scatterers and has a frequency-dependent attenuation of 0.5 dB/cm/MHz. This attenuation was compensated with TGC (time-gain control) in image constructions.

A block diagram of the experiment is shown in Fig. 3. A

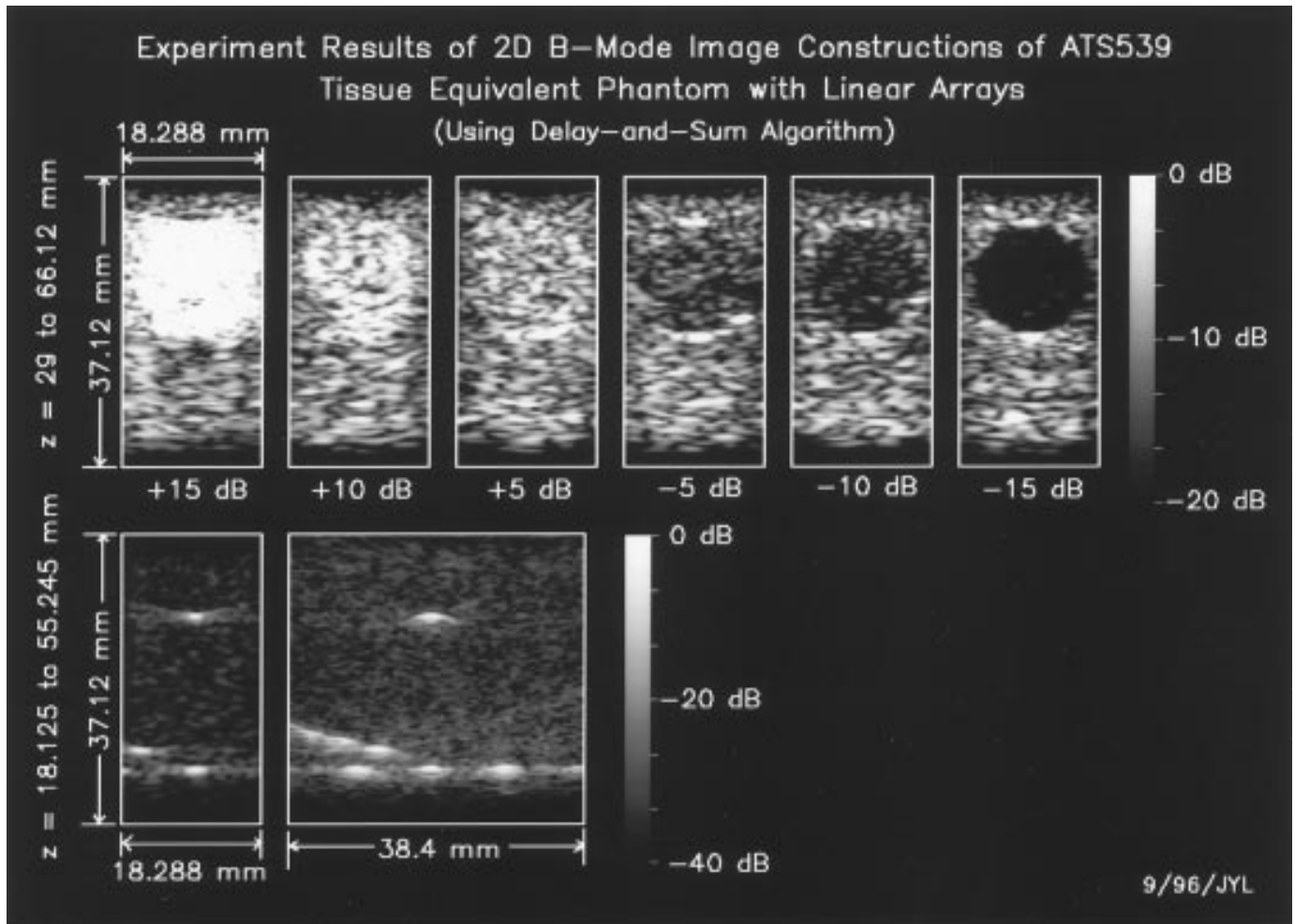


Fig. 5. 2D B-mode images of the ATS539 tissue-equivalent phantom constructed with the same experimental data (plane wave transmission) as those used in Fig. 4 but with the delay-and-sum algorithm (dynamic focusing at each pixel of RF images). The experimental conditions and the format of the figure are the same as that of Fig. 4.

pulser/receiver (Panametrics 5052PR; Panametrics, Inc., Waltham, MA) was used to excite commercial linear array transducers with short (broadband) electric pulses. Echoes from the phantom were received with the same arrays, amplified, low-pass filtered, and digitized (HP E1429A; Hewlett Packard Company, Santa Clara, CA). The system was controlled by a computer (SUN SPARC Station 1; Sun Microsystems Computer Corporation, Mountain View, CA) via a LabView (National Instruments, Austin, TX) driver. To start data acquisition, the computer sent out a signal to activate the counter in the digitizer that in turn produced a synchronized pulse to trigger the pulser to excite transducers to transmit acoustic waves. After a preset delay time (set with the LabView), the digitizer acquired data from the echo signals. The LabView also can be set to average the digitized signals to improve the SNR by repeating the triggering process. The acquired data were then written to a hard disk of the computer.

Two linear array transducers that have no elevation focusing were used for the experiment (the diagrams of the arrays were shown at the lower right of Fig. 4). One has 48 elements, a center frequency of 2.25 MHz, and a di-

mension of 18.288 mm \times 12.192 mm with an inter-element distance of 0.381 mm. The other is a 2.5 MHz array of 64 elements and a dimension of 38.4 mm \times 10 mm with an inter-element space of 0.6 mm. Both arrays have a poor quality. The 48-element array was a product to be thrown away by a commercial company and was a bare bone unit without plastic housing and wire connections. The other was made in the early 1970s, and its pulse-echo sensitivity is about 40 dB lower than the first one. In addition, the 5th and 11th elements of this array were broken. To transmit a plane wave pulse approximately, all array elements were connected together electronically except the one for the receive. This simplified the experiment greatly because no T/R switches were needed. However, this also introduced errors because, for each receive element, the phantom was illuminated with a different transmit wave. Received signals were digitized at a 20 MHz sampling rate and at a 12-bit resolution and were recorded for each element sequentially. For simplicity, all the array elements were untuned. This reduced the fractional bandwidths of the arrays to about 40%. From the experiment data, 2D B-mode images were constructed with the Fourier method (Fig. 4).

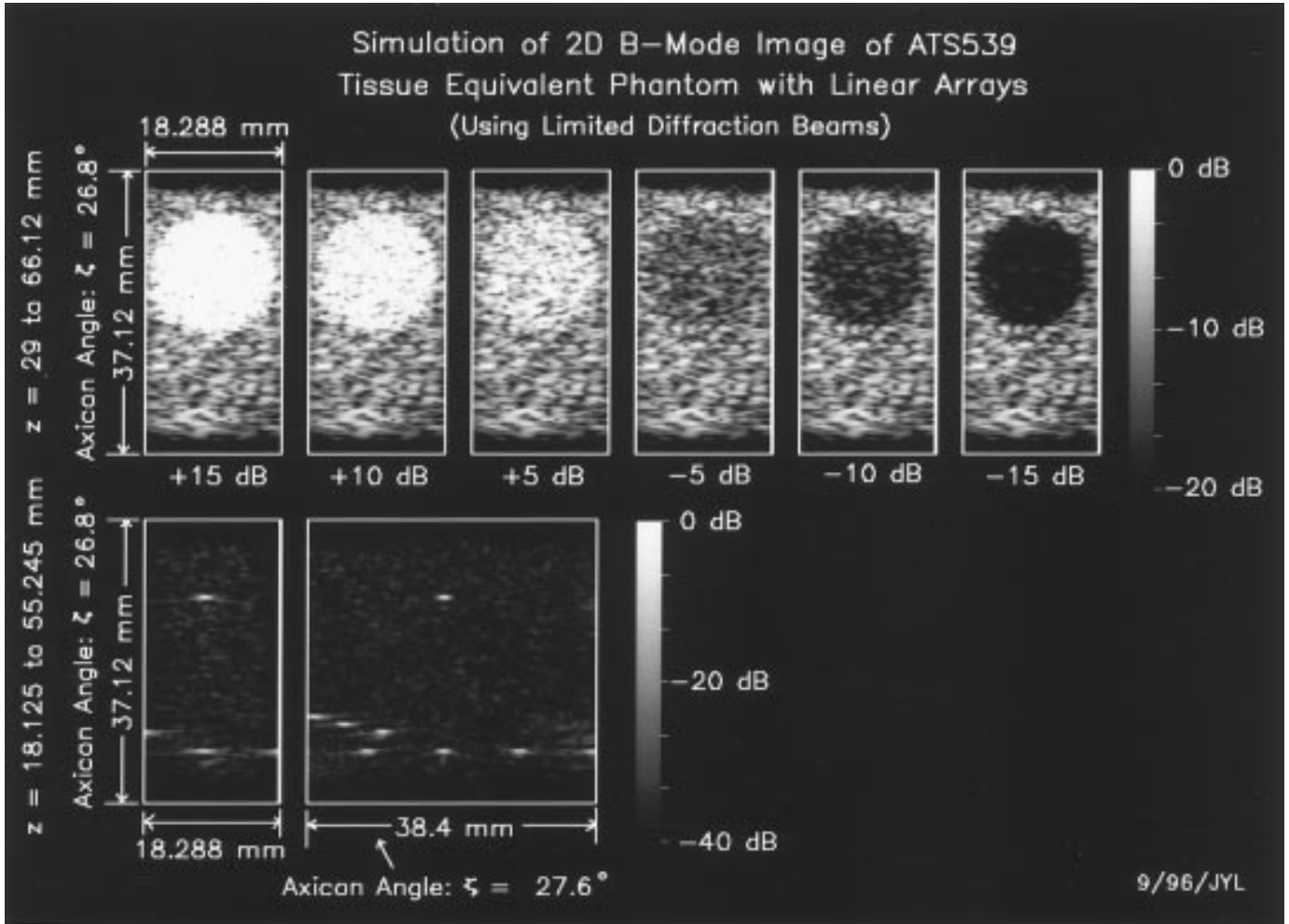


Fig. 6. 2D B-mode images of an ATS539 tissue-equivalent phantom constructed with computer simulation and with the Fourier method. A plane wave pulse is assumed in transmission. The format of the figure is the same as that of Fig. 4.

In Fig. 4, images of a width of 18.288 mm were constructed with the 48-element array and signal from each element was averaged 10 times before the construction. The 64-element array was used to construct images of a width of 38.4 mm and signals were averaged 20 times (Fig. 4). The Axicon angles, ζ , used for the construction are shown in Fig. 4.

For comparison, the same data obtained from the experiment were used to construct images with the delay-and-sum (dynamic focusing) algorithm [39]. Results are shown in Fig. 5. Comparing Fig. 5 with Fig. 4, we see little difference between them except that there are slight artifacts and higher sidelobes in Fig. 5. This means that the two methods are essentially identical. However, as mentioned in the Introduction, the delay-and-sum algorithm requires more computation leading to a complex system.

To see how well the images can be constructed with perfect arrays under ideal conditions required by the theory [(12) or (22)], computer simulations were performed. In the simulation, two linear array transducers that were identical to those for the experiment were used. However, two-way (pulse-echo) spectra of the arrays were assumed to be larger and proportional to the Blackman window

function (14) with a fractional bandwidth of about 81% (typical for a modern array). The object used for the simulation was based on the ATS539 phantom but with no attenuation. The object consisted of wires, cysts, and cylinders of various scattering densities relative to the scattering background (Fig. 2), and their cross-sections were imaged. To construct images, all the array elements were connected together to transmit a pulse (broadband) plane wave (9). Echoes from objects were received with the same array elements but weighted to produce limited diffraction responses (17). The spatial frequencies, k_x , of the weighting functions were chosen at equal-distance intervals for use with the IFFT [see (19) and (22)]. The received signals (A-lines) were digitized and Fourier transformed with FFTs to give Fourier transform of the object function evaluated at the equal-distance interval of k . Given k_x and k_z were calculated with [see (18)]:

$$k'_z = k + k_z = k + \sqrt{k^2 - k_x^2}, \quad (24)$$

where $k = 2\pi f/c$. With the nearest-neighbor interpolation [56], the temporal spectra of the received signals (22) can be obtained at the equal-distance intervals of k'_z . From

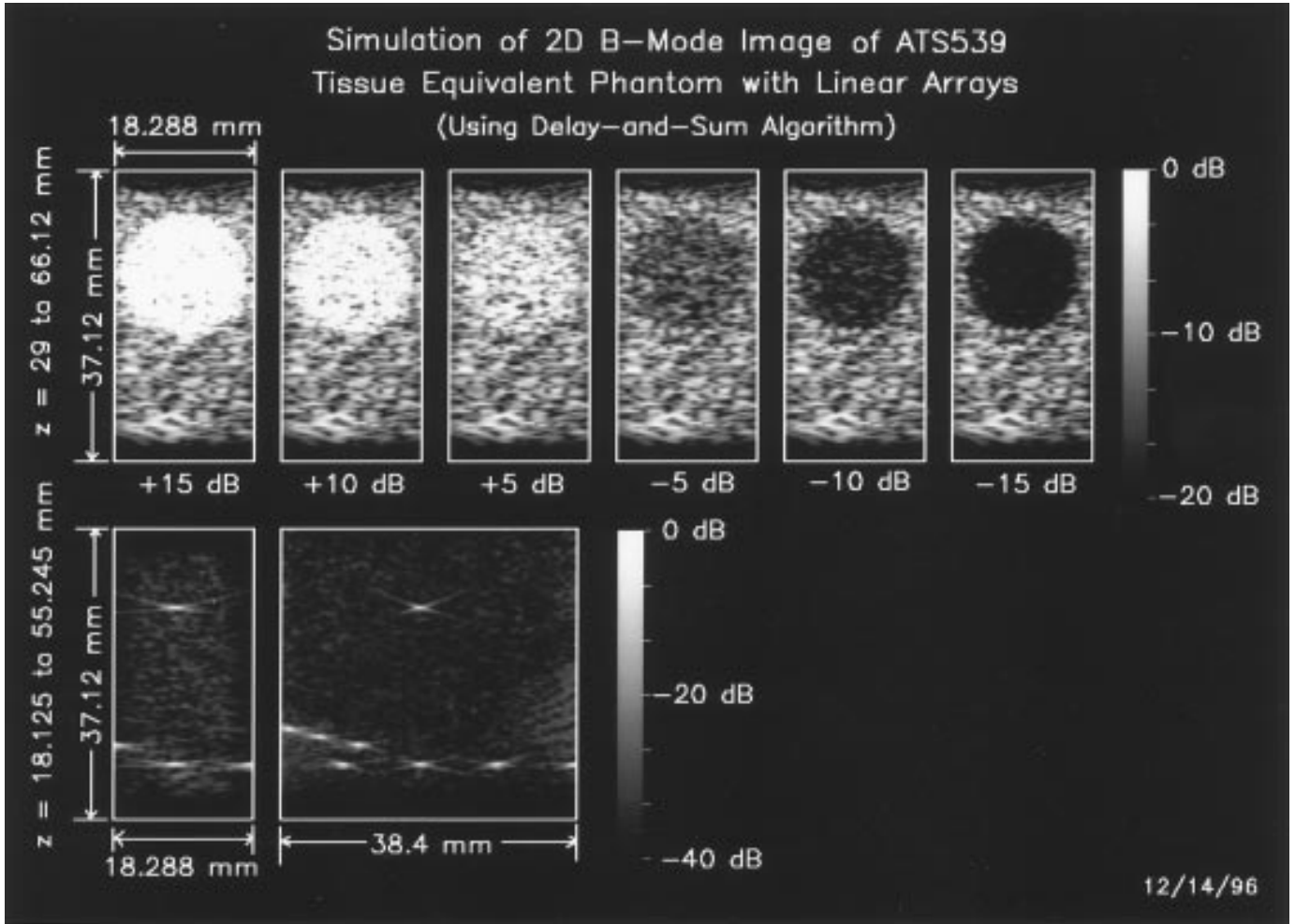


Fig. 7. 2D B-mode images of the ATS539 tissue-equivalent phantom constructed with the same computer simulation data as those used in Fig. 6, but with a delay-and-sum algorithm (dynamic focusing at each pixel of RF images). The simulation conditions and the format of the figure are the same as those of Fig. 6.

the 2D spectra evaluated at rectangular grids, object functions can be constructed directly with a 2D IFFT [(19) and (22)].

Images constructed with the simulation using the Fourier and the conventional dynamic focusing (delay-and-sum) methods are shown in Figs. 6 and 7, respectively. Comparing these images with those in Figs. 4 and 5, we see that they are close except that the resolution in Figs. 4 and 5 is lower. This means that the experiment agrees with the simulation very well, and good images can be constructed with the Fourier method although the experiment are performed under imperfect conditions (insensitive to minor errors). The lower resolution in Figs. 4 and 5 is caused by the smaller bandwidths of the practical transducers.

IV. DISCUSSION

From results of the experiment (Figs. 4 and 5) and computer simulation (Figs. 6 and 7) in the last section, it is clear that the quality (resolution and sidelobe) of images constructed with the Fourier method is almost identical

to that obtained with the conventional dynamic focusing (delay-and-sum) method with the same transmission beam. In the following, features of the Fourier method will be discussed.

A. Production of Limited Diffraction Beams

Limited diffraction weighting: The main difference of the current Fourier method from previous ones [47], [48], [51] is that in the current method, limited diffraction beams are used to construct images. To produce limited diffraction beams, the aperture of a transducer is weighted with simple stepwise sine ($\sin(k_x x + k_y y)$) and cosine ($\cos(k_x x + k_y y)$) functions [(4) and (17)]. This is similar to the production of a Bessel beam where a stepwise Bessel function is used to weight a transducer aperture [8], [9]. The advantages of using limited diffraction beams are that imaging systems are simplified (no delay of either transmit or receive signal is necessary) and the transmission energy can be larger (the entire array aperture is used in both transmit and receive beamforming). In addition, similar to the frequency and phase encoding in MRI (magnetic

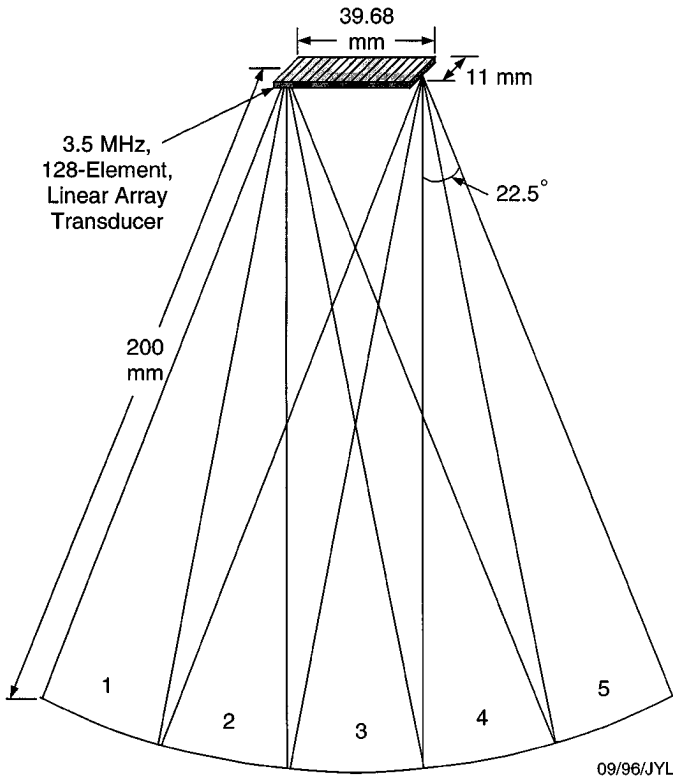


Fig. 8. Electronic steering of a beam at five discrete angles to increase the field of view for the Fourier method.

resonant imaging) [62], [63], the free parameters of limited diffraction beams, k_x and k_y [(4) and (17)], can be easily chosen to produce the spatial Fourier transform of an object function at rectangular grids making it easier for the subsequent spatial IFFT.

Number of elements: The maximum values of k_x and k_y determine the highest lateral resolution of constructed images in the x and y directions, respectively. Because lateral resolution of an imaging system is usually much lower than axial, i.e., $k_x \ll k$ and $k_y \ll k$, the inter-element space of an array transducer can be larger than $\lambda/2$ without aliasing, where λ is the central wavelength. In this case, subdicing techniques used in conventional linear arrays can be applied to reduce grating lobes without increasing the number of individually addressable elements [38]. Therefore, the Fourier method is scaleable, i.e., both fully and under sampled arrays can be used to construct images of a high and low lateral resolution, respectively. Apparently, with an undersampled array, imaging systems can be simplified because the number of array elements, and thus the number of channels, are smaller.

B. High Frame Rate Imaging

High frame rate: Because only one transmission is necessary to construct both 2D and 3D images [(11) and (19)], the highest possible frame rate with the Fourier method is about 3750 frames/s for a depth of 200 mm in biological soft tissues. To achieve this frame rate in a practical system, A-lines must be processed in parallel. A-lines in the

Fourier method are produced with simple stepwise sine and cosine weightings with desired spatial frequencies, k_x and k_y [(4) and (17)] (notice that the A-lines here have a broader meaning and may not necessarily be produced with a thin, focused beam). Each of the A-lines is Fourier transformed to obtain a temporal spectrum [(12) or (22)]. From the spectra of all A-lines, 2D and 3D images are constructed with inverse 2D (22) and 3D (12) spatial Fourier transforms, respectively, after the nearest-neighbor interpolation in the k'_z axis (24) [56]. The Fourier transform for each A-line can be implemented with FFT that can be performed with one or more fast DSP (digital signal processing) chips or an ASIC (application specific integrated circuit). The processing time must be within 267 μ s to achieve the frame rate of 3750 frames/s. Multiple FFT units also can be combined to perform a high-speed 2D or 3D IFFT to construct images within this time slot. Apparently, the more FFT units are in the system, the faster the processing speed will be. The amount of computation for the FFT and IFFT is well known [64], which is much smaller than that required by the dynamic focusing (delay-and-sum) technique, especially, for 3D imaging. This simplifies imaging systems greatly as compared to conventional imaging method attempting to achieve the same frame rate.

Potential for blood flow imaging: Because the Fourier method can achieve an ultrahigh frame rate, it can be used for blood flow vector imaging with speckle tracking techniques [40] without the problem of frame decorrelation. Even with conventional color doppler flow imaging techniques [41], high frame rates will increase the accuracy for flow velocity and volume measurements because more samples are available without noticeably reducing frame rate.

Signal to noise ratio: In the high frame rate Fourier imaging, a broadband plane wave (9) is used to illuminate objects. The plane wave will not diverge over a depth of 200 mm with a conventional medical transducer [18]. This means that the SNR of the imaging systems is high as compared to that of previous methods using diverged beams [47], [50], [51]. Moreover, because the energy density of a plane wave is uniform in transverse directions, a higher total power can be transmitted to further increase the SNR without exceeding the peak power limited by FDA (Food and Drug Administration) regulations. This is also the case when transmit with other types of limited diffraction beams such as the array beams [13], [25], [26].

Field of view and electronic steering of beams: The plane wave transmission may limit the field of view of constructed images because objects that fall outside the projection of the array aperture are not imaged. In cardiac imaging, because the foot print of a transducer is usually small ($< 40 \text{ mm} \times 15 \text{ mm}$), this may cause inconvenience. To increase the field of view, limited diffraction beams can be steered electronically [24]. In this case, image frame rate will be reduced a few folds depending on the size of a viewing area relative to the size of a transducer. For the example shown in Fig. 8, the frame rate

is reduced by 5 folds, i.e., the highest frame rate will be about 750 frames/s. The areas where multiple constructed images overlap can be used for incoherent processing to enhance image contrast (Fig. 8). However, to steer beams electronically, the number of elements in the scan direction must be increased so that the inter-element distance is $\leq \lambda/2$ to avoid grating lobes. This increases system complexity.

C. Transmit-Receive (Two-Way) Beam Forming Without Reducing Frame Rate

Recently, a computer simulation was performed to construct images with two-way beam forming where limited diffraction beams of different parameters are used in both transmission and reception [69]. Field of view, resolution, and sidelobes were studied in detail. The following is a summary of the results.

Large field of view: As mentioned above, plane wave transmission may limit the field of view of an image to the size of the transducer aperture. To increase the field of view without using beam steering, limited diffraction beams of different parameters can be used in both transmission and reception. Because multiple transmissions are necessary to construct a frame of image, the frame rate of this method is low, especially for 3D imaging. Low frame rates will make flow vector imaging difficult. However, a low frame rate allows more time to process signals and thus fewer parallel processing units are needed and imaging systems can be further simplified.

Large Fourier-domain coverage: With limited diffraction beams in both transmission and reception, the Fourier-domain coverage increases (see equation 42 and Fig. 13 in [38]). This increases lateral resolution of constructed images.

Cosine shading: High-resolution and low-sidelobe images can be constructed when limited diffraction beams are used in both transmission and reception, and a cosine shading is applied to both transmit and receive apertures. To achieve the same high resolution and low sidelobe with conventional dynamic focusing methods, in addition to the cosine aperture shading, multiple frames of images should be combined with a montage. The montage process further lowers image frame rates. In addition, dynamic focusing requires more computation leading to complex systems.

D. Image Contrast

From the above discussion, it is clear that, to achieve a high frame rate, a broad illumination beam has to be used to allow parallel receive beamforming. This reduces image contrast (see Figs. 4, 5, 6, and 7). Fortunately, high frame rate imaging is usually used for fast moving objects such as the heart leaflet that enhances the visual contrast because of the motion. For slow moving objects such as liver and kidney, two-way Fourier method can be used to obtain high resolution and high contrast images at a lower frame rate.

E. Phase Aberration and Nonuniform Frequency-Dependent Attenuation

For any beamforming techniques to work properly, the media in which beams propagate must be free from phase aberration and nonuniform frequency-dependent attenuation. However, this is not true in biological soft tissues. These imperfect conditions will cause beam distortion leading to a poor image quality. The influence of the phase aberration on the Fourier method has been studied recently. Results show that the phase aberration has similar effects on both the Fourier and conventional dynamic focusing methods [42]. Methods for reducing phase aberration in conventional B-scan imaging have been developed by many research groups [65]–[68]. These methods are also applicable to the Fourier method.

Frequency-dependent attenuation can be compensated with a TGC (time-gain control) as is shown in the experiment. However, nonuniform attenuation along depth direction may be difficult to compensate.

V. CONCLUSION

A new image construction method (Fourier method) has been developed with limited diffraction beams. This method has several important features: high frame rate, high SNR, can be implemented with simple and inexpensive hardware, and high quality (high resolution and low sidelobe) that are comparable to conventional dynamic focusing systems when using the same transmission beams. Theory, computer simulation, and experiment of the method have been performed, and they agree very well with each other. This method may result in a new generation of ultrasound imager that has a higher medical diagnostic potential but a lower cost.

ACKNOWLEDGMENTS

The author thanks Dr. James F. Greenleaf in the Department of Physiology and Biophysics, Mayo Clinic, for useful discussions. The author also appreciates Mr. Randall R. Kinnick for making connectors of the 1D linear arrays and Mr. Thomas M. Kinter for making a LabView program for data acquisition in the experiment.

REFERENCES

- [1] J. A. Stratton, *Electromagnetic Theory*. New York: McGraw-Hill, 1941, p. 356.
- [2] J. Durnin, "Exact solutions for nondiffracting beams. I. The scalar theory," *J. Opt. Soc. Amer. A*, vol. 4, no. 4, pp. 651–654, 1987.
- [3] J. Durnin, J. J. Miceli, Jr., and J. H. Eberly, "Diffraction-free beams," *Phys. Rev. Lett.*, vol. 58, pp. 1499–1501, Apr. 13, 1987.
- [4] A. Vasara, J. Turunen, and A. T. Friberg, "Realization of general nondiffracting beams with computer-generated holograms," *J. Opt. Soc. Amer. A*, vol. 6, pp. 1748–1754, Nov. 1989.

- [5] J. Ojeda-Castaneda and A. Noyola-Iglesias, "Nondiffracting wavefields in grin and free-space," *Microwave Opt. Technol. Lett.* vol. 3, pp. 430–433, Dec. 1990.
- [6] D. K. Hsu, F. J. Margetan, and D. O. Thompson, "Bessel beam ultrasonic transducer: fabrication method and experimental results," *Appl. Phys. Lett.*, vol. 55, pp. 2066–2068, Nov. 13, 1989.
- [7] J. A. Campbell and S. Soloway, "Generation of a nondiffracting beam with frequency independent beam width," *J. Acoust. Soc. Amer.*, vol. 88, pp. 2467–2477, Nov. 1990.
- [8] J.-y. Lu and J. F. Greenleaf, "Ultrasonic nondiffracting transducer for medical imaging," *IEEE Trans. Ultrason., Ferroelect., Freq. Contr.*, vol. 37, pp. 438–447, Sept. 1990.
- [9] —, "Pulse-echo imaging using a nondiffracting beam transducer," *Ultrason. Med. Biol.*, vol. 17, pp. 265–281, May 1991.
- [10] —, "Diffraction-limited beams and their applications for ultrasonic imaging and tissue characterization," in *New Developments in Ultrasonic Transducers and Transducer Systems*, F. L. Lizzi, Ed., *Proc. SPIE*, vol. 1733, pp. 92–119, 1992.
- [11] —, "Formation and propagation of limited diffraction beams," in *Acoust. Imaging*, vol. 20, pp. 331–343, 1993.
- [12] —, "Evaluation of a nondiffracting transducer for tissue characterization," *Proc. IEEE Ultrason. Symp.*, vol. 2, 1990, pp. 795–798.
- [13] J.-y. Lu, "Limited diffraction array beams," *Int. J. Imaging Syst. Technol.*, vol. 8, pp. 126–136, Jan. 1997.
- [14] J.-y. Lu, "Improving accuracy of transverse velocity measurement with a new limited diffraction beam," *Proc. IEEE Ultrason. Symp.*, vol. 2, 1996, pp. 1255–1260.
- [15] J.-y. Lu, X.-L. Xu, H. Zou, and J. F. Greenleaf, "Application of Bessel beam for doppler velocity estimation," *IEEE Trans. Ultrason., Ferroelect., Freq. Contr.*, vol. 42, pp. 649–662, July 1995.
- [16] J.-y. Lu, "High-speed transmissions of images with limited diffraction beams," in *Acoustical Imaging*, vol. 23 (in press).
- [17] J.-y. Lu and J. F. Greenleaf, "Producing deep depth of field and depth-independent resolution in NDE with limited diffraction beams," *Ultrason. Imaging*, vol. 15, pp. 134–149, Apr. 1993.
- [18] —, "Nondiffracting X waves—exact solutions to free-space scalar wave equation and their finite aperture realizations," *IEEE Trans. Ultrason., Ferroelect., Freq. Contr.*, vol. 39, pp. 19–31, Jan. 1992.
- [19] —, "Experimental verification of nondiffracting X waves," *IEEE Trans. Ultrason., Ferroelect., Freq. Contr.*, vol. 39, pp. 441–446, May 1992.
- [20] J.-y. Lu, T. K. Song, R. R. Kinnick, and J. F. Greenleaf, "In vitro and in vivo real-time imaging with ultrasonic limited diffraction beams," *IEEE Trans. Med. Imag.*, vol. 12, pp. 819–829, Dec. 1993.
- [21] J.-y. Lu, H. Zou, and J. F. Greenleaf, "Biomedical ultrasound beamforming," *Ultrason. Med. Biol.*, vol. 20, pp. 403–428, July 1994.
- [22] J.-y. Lu, M. Fatemi, and J. F. Greenleaf, "Pulse-echo imaging with X wave," *Acoust. Imaging*, vol. 22, pp. 191–196, 1996.
- [23] T. K. Song, J.-y. Lu, and J. F. Greenleaf, "Modified X waves with improved field properties," *Ultrason. Imaging*, vol. 15, pp. 36–47, Jan. 1993.
- [24] J.-y. Lu and J. F. Greenleaf, "A study of two-dimensional array transducers for limited diffraction beams," *IEEE Trans. Ultrason., Ferroelect., Freq. Contr.*, vol. 41, pp. 724–739, Sept. 1994.
- [25] J.-y. Lu, "Construction of limited diffraction beams with Bessel bases," *Proc. IEEE Ultrason. Symp.*, vol. 2, 1995, pp. 1393–1397.
- [26] —, "Designing limited diffraction beams," *IEEE Trans. Ultrason., Ferroelect., Freq. Contr.*, vol. 44, pp. 181–193, Jan. 1997.
- [27] J.-y. Lu, H. Zou, and J. F. Greenleaf, "A new approach to obtain limited diffraction beams," *IEEE Trans. Ultrason., Ferroelect., Freq. Contr.*, vol. 42, pp. 850–853, Sept. 1995.
- [28] J.-y. Lu and J. F. Greenleaf, "Sidelobe reduction for limited diffraction pulse-echo systems," *IEEE Trans. Ultrason., Ferroelect., Freq. Contr.*, vol. 40, pp. 735–746, Nov. 1993.
- [29] —, "Sidelobe reduction of nondiffracting pulse-echo images by deconvolution," *Ultrason. Imaging*, vol. 14, p. 203, Apr. 1992 (Abstr.).
- [30] J.-y. Lu, "Bowtie limited diffraction beams for low-sidelobe and large depth of field imaging," *IEEE Trans. Ultrason., Ferroelect., Freq. Contr.*, vol. 42, pp. 1050–1063, Nov. 1995.
- [31] —, "Producing bowtie limited diffraction beams with synthetic array experiment," *IEEE Trans. Ultrason., Ferroelect., Freq. Contr.*, vol. 43, pp. 893–900, Sept. 1996.
- [32] J. N. Brittingham, "Focus wave modes in homogeneous Maxwell's equations: transverse electric mode," *J. Appl. Phys.*, vol. 54, no. 3, pp. 1179–1189, 1983.
- [33] R. W. Ziolkowski, "Exact solutions of the wave equation with complex source locations," *J. Math. Phys.*, vol. 26, pp. 861–863, Apr. 1985.
- [34] R. W. Ziolkowski, D. K. Lewis, and B. D. Cook, "Evidence of localized wave transmission," *Phys. Rev. Lett.*, vol. 62, pp. 147–150, Jan. 9, 1989.
- [35] E. Heyman, B. Z. Steinberg, and L. B. Felsen, "Spectral analysis of focus wave modes," *J. Opt. Soc. Amer. A*, vol. 4, pp. 2081–2091, Nov. 1987.
- [36] R. Donnelly, D. Power, G. Templeman, and A. Whalen, "Graphic simulation of superluminal acoustic localized wave pulses," *IEEE Trans. Ultrason., Ferroelect., Freq. Contr.*, vol. 41, pp. 7–12, Jan. 1994.
- [37] J.-y. Lu and J. F. Greenleaf, "Comparison of sidelobes of limited diffraction beams and localized waves," *Acoust. Imaging*, vol. 21, pp. 145–152, 1995.
- [38] J.-y. Lu, "2D and 3D high frame rate imaging with limited diffraction beams," *IEEE Trans. Ultrason., Ferroelect., Freq. Contr.*, vol. 14, no. 4, Jul. 1997, pp. 839–856.
- [39] J. Shen, H. Wang, C. Cain, and E. S. Ebbini, "A post-beamforming processing technique for enhancing conventional pulse-echo ultrasound imaging contrast resolution," *Proc. IEEE Ultrason. Symp.*, vol. 2, 1995, pp. 1319–1322.
- [40] G. E. Trahey, S. M. Hubbard, and O. T. von Ramm, "Angle independent ultrasonic blood flow detection by frame-to-frame correlation of B-mode images," *Ultrasonics*, vol. 26, pp. 271–276, 1988.
- [41] K. Miyatake, M. Okamoto, N. Kinoshita, S. Izumi, M. Owa, S. Takao, H. Sakakibara, and Y. Nimura, "Clinical applications of a new type of real-time two-dimensional doppler flow imaging system," *Amer. J. Cardiol.*, vol. 54, pp. 857–868, 1984.
- [42] J.-y. Lu, "Assessment of phase aberration effects on high frame rate imaging," *Ultrason. Imaging*, vol. 19, pp. 53, January 1997 (Abstr.).
- [43] D. P. Shattuck, M. D. Weinschenker, S. W. Smith, and O. T. von Ramm, "Explososcan: A parallel processing technique for high speed ultrasound imaging with linear phased arrays," *J. Acoust. Soc. Amer.*, vol. 75, no. 4, pp. 1273–1282, 1984.
- [44] S. W. Smith, H. G. Pavy, Jr., and O. T. von Ramm, "High-speed ultrasound volumetric imaging system—Part I: Transducer design and beam steering," *IEEE Trans. Ultrason., Ferroelect., Freq. Contr.*, vol. 38, pp. 100–108, Mar. 1991.
- [45] O. T. von Ramm, S. W. Smith, and H. G. Pavy, Jr., "High-speed ultrasound volumetric imaging system—Part II: Parallel processing and image display," *IEEE Trans. Ultrason., Ferroelect., Freq. Contr.*, vol. 38, pp. 109–115, Mar. 1991.
- [46] P. N. T. Wells, *Biomedical Ultrasonics*. New York: Academic Press, chapters 2–6, 1977.
- [47] J. T. Ylitalo and H. Ermert, "Ultrasound synthetic aperture imaging: monostatic approach," *IEEE Trans. Ultrason., Ferroelect., Freq. Contr.*, vol. 41, pp. 333–339, May 1994.
- [48] M. Soumekh, "Array imaging with beam-steered data," *IEEE Trans. Image Processing*, vol. 1, pp. 379–390, July 1992.
- [49] E. S. Ebbini, "Optimal transversal filter bank for 3D real-time acoustical imaging," *Twenty-Sixth Asilomar Conf. Signals, Syst. Comput.*, vol. 2, pp. 831–835, 1992.
- [50] J. Shen and E. S. Ebbini, "A new coded-excitation ultrasound imaging system—Part I: Basic principles," *IEEE Trans. Ultrason., Ferroelect., Freq. Contr.*, vol. 43, pp. 131–140, Jan. 1996.
- [51] S. J. Norton and M. Linzer, "Ultrasonic reflectivity imaging in three dimensions: exact inverse scattering solutions for plane, cylindrical, and spherical apertures," *IEEE Trans. Biomed. Eng.*, vol. BME-28, pp. 202–220, Feb. 1981.
- [52] D. Hiller and H. Ermert, "System analysis of ultrasound reflection mode computerized tomography," *IEEE Trans. Sonics Ultrason.*, vol. SU-31, pp. 240–250, July 1984.
- [53] B. A. Roberts and A. C. Kak, "Reflection mode diffraction tomography," *Ultrason. Imaging*, vol. 7, pp. 300–320, Oct. 1985.
- [54] S. A. Johnson, J. F. Greenleaf, M. Tanaka, B. Rajagopalan, and R. C. Bahn, "Reflection and transmission techniques for

- high resolution quantitative synthesis of ultrasound parameter images," *Proc. IEEE Ultrason. Symp.*, 1977, pp. 983–988.
- [55] J. F. Greenleaf and R. C. Bahn, "Clinical imaging with transmissive ultrasonic computerized tomography," *IEEE Trans. Biomed. Eng.*, vol. BME-28, pp. 177–185, Feb. 1981.
- [56] J.-y. Lu, "A computational study for synthetic aperture diffraction tomography: Interpolation versus interpolation-free," *Acoust. Imaging*, vol. 16, pp. 421–443, 1988.
- [57] J. H. Mcleod, "The Axicon: a new type of optical element," *J. Opt. Soc. Amer.*, vol. 44, pp. 592–597, Aug. 1954.
- [58] C. B. Burckhardt, H. Hoffmann, and P. A. Grandchamp, "Ultrasound axicon: a device for focusing over a large depth," *J. Acoust. Soc. Amer.*, vol. 54, pp. 1628–1630, Dec. 1973.
- [59] F. S. Foster, M. S. Patterson, M. Arditi, J. W. Hunt, "The conical scanner: a two transducer ultrasound scatter imaging technique," *Ultrason. Imaging*, vol. 3, no. 1, pp. 62–82, 1981.
- [60] P. M. Morse and H. Feshbach, *Methods of Theoretical Physics, Part I*. New York: McGraw-Hill, 1953, chapter 5.
- [61] R. Bracewell, *The Fourier Transform and Its Applications*. New York: McGraw-Hill, 1965, pp. chapters 4 and 6.
- [62] D. R. Bailes and D. J. Bryant, "NMR imaging," *Contemp. Phys.*, vol. 25, pp. 441–475, 1984.
- [63] M. J. Bronskill and P. Sprawls, *The Physics of MRI—1992 AAPM Summer School Proceedings*. Woodbury, NY: American Institute of Physics, 1993.
- [64] A. V. Oppenheim and R. W. Schaffer, *Digital Signal Processing*. Englewood Cliffs, NJ: Prentice-Hall, 1975, pp. chapters 1 and 5.
- [65] F. S. Foster, and J. W. Hunt, "The focusing of ultrasound beams through human tissue," *Acoust. Imaging*, vol. 8, pp. 709–718, 1979.
- [66] M. O'Donnell and S. W. Flax, "Phase aberration measurements in medical ultrasound: human studies," *Ultrason. Imaging*, vol. 10, pp. 1–11, 1988.
- [67] R. C. Waag, D. Dalecki, and W. A. Smith, "Estimates of wavefront distortion from measurements of scattering by model random media and calf liver," *J. Acoust. Soc. Amer.*, vol. 85, pp. 406–415, 1988.
- [68] G. E. Trahey, P. D. Freiburger, L. F. Nock, and D. C. Sullivan, "In vivo measurements of ultrasonic beam distortion in the breast," *Ultrason. Imaging*, vol. 13, pp. 71–90, 1991.
- [69] Jiay-yu Lu, "Transmit-receive dynamic focusing with limited diffraction beams", IEEE 1997 Ultrasonics Symposium proceedings (In Press).



Jian-yu Lu (M'88) was born in Fuzhou, Fujian Province, People's Republic of China. He received the B.S. degree in electrical engineering in February, 1982 from Fudan University, Shanghai, China; the M.S. degree in 1985 from Tongji University, Shanghai, China; and the Ph.D. degree in 1988 from Southeast University, Nanjing, China.

He is currently a professor in the Department of Bioengineering at The University of Toledo, Toledo, OH. Before joining The University of Toledo in September, 1997, he was an associate professor of Biophysics at the Mayo Medical School and an associate consultant at the Department of Physiology and Biophysics, Mayo Clinic/Foundation, Rochester, MN. From March 1990 to December 1991, he was a research associate at the Department of Physiology and Biophysics, and from December 1988 to February 1990, he was a postdoctoral research fellow there. Prior to that, he was a faculty member of the Department of Biomedical Engineering, Southeast University, Nanjing, China, and worked with Prof. Yu Wei. His research interests are in acoustic imaging and tissue characterization, medical ultrasonic transducers, and ultrasonic beam forming and propagation.

Dr. Lu is a recipient of the Outstanding Paper Award for two papers published in the 1992 *IEEE Transactions* on the UFFC, the recipient of the Edward C. Kendall Award from the Mayo Alumni Association, Mayo Foundation in 1992. He also received both the FIRST Award from the NIH and the Biomedical Engineering Research Grant Award from the Whitaker Foundation in 1991. He is a member of the IEEE UFFC Society, the American Institute of Ultrasound in Medicine, and Sigma Xi.